CHEMISTRY OF MATERIALS
ARTICLE
pubs.acs.org/cm

Phase Behavior of Ionic Liquid−LiX Mixtures: Pyrrolidinium Cations and TFSI$^-$ Anions – Linking Structure to Transport Properties

Qian Zhou,[†] Paul D. Boyle,[‡] Luciana Malpezzi,[§] Andrea Mele,[§] Joon-Ho Shin,[⊥] Stefano Passerini,[⊥,#] and Wesley A. Henderson*[,†]

[†]Ionic Liquids & Electrolytes for Energy Technologies (ILEET) Laboratory, Department of Chemical & Biomolecular Engineering, and [‡]X-ray Structural Facility, Department of Chemistry, North Carolina State University, Raleigh, North Carolina 27695, United States
[§]Department of Chemistry, Materials and Chemical Engineering "G. Natta", Politecnico di Milano, 20131 Milan, Italy
[⊥]Italian National Agency for New Technologies, Energy, and the Environment (ENEA), Casaccia Research Center, 00060 Rome, Italy
[#]Institute of Physical Chemistry, University of Muenster, D 48149 Muenster, Germany

Supporting Information

ABSTRACT: The thermal phase behavior and ionic conductivity of mixtures of *N*-alkyl-*N*-methylpyrrolidinium bis(trifluoromethanesulfonyl)imide ionic liquids ($PY_{1R}TFSI$ where $R = 4$ or 5 for butyl or pentyl) with LiTFSI have been examined as model systems for ionic liquid-based lithium battery electrolytes. Several mixed salt crystalline phases form. The ionic conductivity variability of the mixtures correlates well with the reported phase behavior. The crystal structures for the (1-x) $PY_{1R}TFSI$-(x) LiTFSI ($x = 0.67$) (or 1/2 $PY_{1R}TFSI$/LiTFSI with $R = 4$ or 5) phases have been determined. These phases are isostructural, consisting of ionic planar layers formed by $Li^+\cdots TFSI^-$ linkages in which the uncoordinated PY_{1R}^+ cations reside in cavities within the layers. These structures have been used to aid in correlating Raman data with cation−anion coordination in the IL-LiTFSI binary salt mixtures.

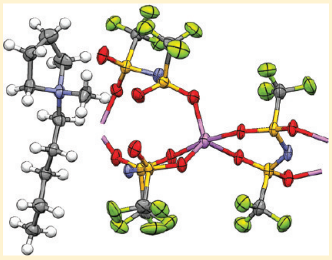

KEYWORDS: ionic liquid, battery electrolyte, lithium, LiTFSI, phase behavior

INTRODUCTION

There is a rapidly expanding interest in using ionic liquids (ILs) as electrolyte materials for electrochemical applications.[1,2] ILs are salts, or mixtures of salts, that melt at low temperature, often below room temperature. The field of ILs has been expanding at a tremendous rate with thousands of papers published over the past several years, whereas only a few dozen were published a decade or more ago. How IL ions interact with solutes and other ions is a key focus for many of the diverse applications suggested/demonstrated for these materials. Further, there is also a recent tremendous renewal of interest in battery materials, especially electrolytes, for electric and plug-in hybrid electric vehicle (EV and PHEV) applications. Current state-of-the-art Li-ion battery electrolytes, composed of a mixture of carbonate solvents and $LiPF_6$,[3] are not suitable for large format battery packs (because of limitations in thermal stability and safety concerns), nor are they useful for the wide range of new high-voltage electrode materials that are a core focus of the battery community. New solvents and salts are needed for electrolyte formulations for advanced batteries. ILs have garnered much attention as electrolyte components due to their exceptional electrochemical stability and low to negligible flammability—they are thus one of only a very few classes of materials that may meet the stringent requirements for new battery electrolytes for Li-ion, Li-metal, and Li-air batteries.

For Li battery electrolyte applications, ILs must be doped with a suitable lithium salt to add electroactive Li^+ cations to the electrolyte for the battery reaction. ILs with *N*-alkyl-*N*-methylpyrrolidinium (PY_{1R}^+) cations and the bis(trifluoromethanesulfonyl)imide ($TFSI^-$) anion, in particular, have been demonstrated as promising electrolytes for Li batteries.[4−10] Despite numerous studies,[11−20] however, the phase behavior and transport properties of (1−x) $PY_{1R}TFSI$-(x) LiTFSI mixtures are not yet well understood. Binary mixtures of LiTFSI with $PY_{1R}TFSI$ ($R = 4$ or 5) have therefore been examined here to add additional insight into the molecular interactions which govern the properties of such mixed-salt electrolytes.

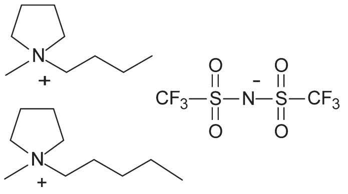

Received: May 19, 2011
Revised: August 4, 2011
Published: September 14, 2011

EXPERIMENTAL SECTION

Materials. 1-Methylpyrrolidine (97%), 1-iodobutane (99%), and 1-iodopentane (98%) were purchased from Aldrich and used as-received. LiTFSI was purchased from 3 M and dried under vacuum at 120 °C for 12 h before use.

Sample Preparation. $PY_{14}TFSI$ was prepared by a procedure reported in the literature.[21] $PY_{15}TFSI$ was prepared by the following related procedure: *N*-methyl-*N*-pentylpyrrolidinium iodide was first prepared by combining 1-methylpyrrolidine with a stoichiometric amount of 1-iodopentane in ethyl acetate (Aldrich). The resulting white crystalline $PY_{15}I$ salt was repeatedly washed using ethyl acetate and then dissolved in deionized water. A stoichiometric amount of LiTFSI dissolved in deionized water was added and the mixture was stirred. Upon standing, two liquid layers form. The top aqueous phase with dissolved LiI was removed, and the remaining IL (i.e., $PY_{15}TFSI$) was washed 8 times with deionized water to ensure the complete removal of reagents and contaminants. The final aqueous layer was removed and the IL was heated while stirring on a hot plate for several hrs. at 120−140 °C to remove most of the residual water. Activated carbon (Darco-G60, Aldrich) was added and the slurry was stirred on a hot plate at 140 °C for 48 h. The slurry was then cooled to room temperature, ethyl acetate was added to dilute the IL and the resulting mixture was filtered through an activated alumina (acidic, Brockmann I, Aldrich) column. The ethyl acetate was removed using a rotary evaporator and the IL was dried under high vacuum at 120 °C overnight and then at 140 °C for another 8 h. After purification and drying, the IL was a clear, colorless liquid at room temperature. The IL was stored in a hermetically sealed bottle in a Vacuum Atmospheres N_2 glovebox (water concentration <0.5 ppm).

Mixed salt samples, $(1-x)$ $PY_{1R}TFSI$-(x) LiTFSI (x is the mole fraction, $R = 4$ or 5), were prepared in the glovebox by combining appropriate amounts of the $PY_{1R}TFSI$ and LiTFSI salts in vials and then heated on a hot plate while stirring to form homogeneous mixtures. The resulting IL-LiX mixtures were clear and colorless with a moisture content below 10 ppm (tested by Karl Fischer titration). The samples were stored in hermetically sealed glass vials in the glovebox.

Thermal Measurements. Thermal measurements were performed using a TA Instruments Q2000 differential scanning calorimeter (DSC) with liquid N_2 cooling. The instrument was calibrated with cyclohexane (solid−solid phase transition at −87.06 °C, melt transition at 6.54 °C) and indium (melt transition at 156.60 °C). Hermetically sealed Al sample pans were prepared in the glovebox. Typically, sample pans were slowly cooled (5 °C min^{-1}) to −150 °C and then heated (5 °C min^{-1}) to various temperatures to ensure the complete crystallization of the samples. After crystallization, the samples were cooled to −150 °C, followed by heating to 100 °C or higher (determined by the composition of the sample) (5 °C min^{-1}) for the final measurements reported. Temperatures noted are for peak temperatures.

Ionic Conductivity. The ionic conductivity was measured using an AMEL Instruments 160 conductivity meter. The samples (3−5 g each) were placed in glass vials, conductivity cells were added and the vial caps were hermetically sealed using an O-ring and Parafilm. The hermetically sealed sample vials were stored in a freezer overnight to fully crystallize the samples. The vials were then placed in a cooling bath at −25 °C. The temperature was changed in 2.5 °C increments and the samples were equilibrated at each temperature for approximately 25−30 min. Conductivity values was measured while heating from −25 to 92.5 °C.

X-ray Structural Determination. (North Carolina State University) Single crystals of the 1/2 ($x = 0.67$) $PY_{15}TFSI$/LiTFSI phase formed in the $x = 0.45$ sample vial after storage at room temperature. A crystal was mounted on a nylon loop with a small amount of Paratone N oil. Data were collected on a Bruker-Nonius Kappa Axis X8 Apex2 diffractometer at a temperature of −163 °C using Mo−Kα radiation. The unit cell dimensions were determined from a symmetry constrained fit of 9914 reflections with $4.82° \leq 2\theta \leq 50.0°$. The data collection strategy was a number of ω and φ scans which collected data up to 50.26° (2θ). The frame integration was performed using SAINT.[22] The resulting raw data was scaled and absorption corrected using a multiscan averaging of symmetry equivalent data using SADABS.[22] The structure was solved by direct methods using the XM program.[22] Most non-hydrogen atoms were obtained from the initial solution. The remaining non-hydrogen atomic positions were derived from subsequent difference Fourier maps. The independent part of the unit cell contains 24 ions: eight Li^+ cations, four $PY_{15}{}^+$ cations, and 12 $TFSI^-$ anions. The structural model was fit to the data using full matrix least-squares based on F^2. The calculated structure factors included corrections for anomalous dispersion from the usual tabulation. The structure was refined using the XL program from SHELXTL.[22] Crystallographic figures were drawn using Mercury 2.2 and Ortep-3 software.

(Politecnico di Milano): A crystal of the 1/2 ($x = 0.67$) $PY_{14}TFSI$/LiTFSI phase was selected from the semisolid mixture in a $x = 0.40$ sample vial after storage at room temperature. The crystal was fixed on a glass fiber with Galden oil and mounted on the diffractometer under a nitrogen flux at −180 °C. X-ray measurements were made on a Bruker-Nonius Kappa Axis X8 Apex2 diffractometer at a temperature of −163 °C using Mo−Kα radiation. Unit-cell dimensions were calculated from least-squares refinement of 20449 reflections with $2.2° \leq 2\theta \leq 50.0°$. A total of 62206 reflections was collected, corresponding to 25449 unique reflections. Raw intensity data were corrected for absorption using SADABS.[22] The structure was solved by direct methods using SIR97.[23] Many atoms were obtained from the initial solution. The other non-hydrogen atoms were found from successive difference Fourier maps using SHELXTL.[24] The independent part of the unit cell contains 24 ions: 8 Li^+ cations, 4 $PY_{14}{}^+$ cations and 12 $TFSI^-$ anions. During refinement, significant disorder of several units was observed in the crystal structure. The final disordered model has been obtained using two different procedures: (i) a single $PY_{14}{}^+$ unit (U named unit), with orientational disorder lying across an inversion center, was refined with all the constraints needed to satisfy this geometry and (ii) the atoms of the other disordered units were refined isotropically and left free from constraints in the last cycles of refinement. All hydrogen atoms were introduced at calculated positions and allowed to ride on the parent atoms. The final stage of refinement used full matrix least-squares based on F^2. Crystallographic figures were drawn using Mercury 2.2 software.

Raman Measurement. Raman spectra were collected from −150 to 100 °C with a Jobin-Yvon LabRAM HR800 spectrometer. Spectra were excited with the 632.8 nm line of a HeNe internal laser. The measurement time was 10 s with five accumulations. For the measurements, the samples were placed in a cavity on a stainless steel plate in a hermetically sealed Linkam LTS350 heating/cooling stage in the glovebox. The stage was then transferred to the spectrometer and Raman spectra were measured over the frequency range 100−1800 cm^{-1}. The spectra were normalized by integrating the intensity of the most intense Raman band between 785 and 690 cm^{-1}.

RESULTS AND DISCUSSION

Phase Behavior. DSC heating traces for the $(1-x)$ $PY_{14}TFSI$-(x) LiTFSI mixtures have been previously reported.[17] The data for $(1-x)$ $PY_{1R}TFSI$-(x) LiTFSI mixtures are shown in Figure 1. The neat $PY_{15}TFSI$ salt has relatively simple phase behavior with a single melting endotherm noted ($T_m = 10$ °C). That is one reason why this salt was selected for study, as the neat $PY_{13}TFSI$ and $PY_{14}TFSI$ salts have more complicated phase behavior due to the formation of polymorphic crystalline phases.[17] Upon the addition of small amounts of LiTFSI, the mixtures melt at a slightly lower temperature than for the neat IL because of the formation of a eutectic phase. The data indicate that both $x = 0.33$ ($T_m = 28$ °C, 2/1 IL/LiX) and 0.67 ($T_m = 76$ °C, 1/2 IL/LiX) phases form in common with similar

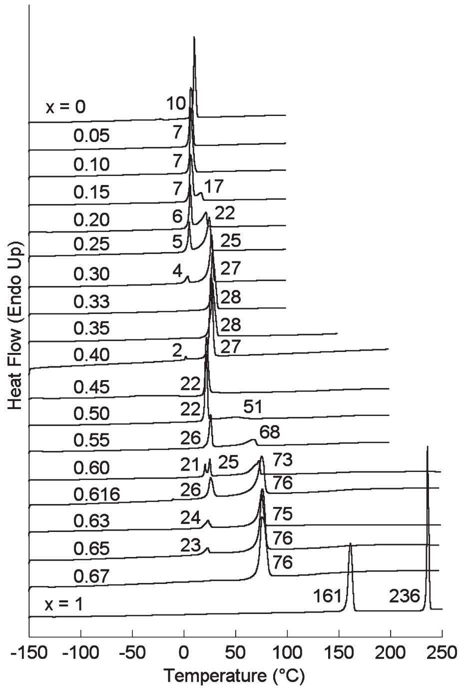

Figure 1. DSC heating traces (5 °C min^{-1}) of (1-x) PY_{15}TFSI-(x) LiTFSI mixtures (peak temperatures and composition noted).

mixtures with PY_{1R}TFSI (R = 2−4) ILs.[17] The mixtures also show variable phase behavior near x = 0.50 suggesting that a 1/1 IL/LiX metastable, polymorphic phase (T_m = 22 °C) may also form. An alternative explanation for the observed peak at 22 °C may be due to the melting of a eutectic composition between the x = 0.33 and 0.67 phases. This peak is not found to be consistently reproducible in repeated heating/cooling traces as its formation appears to be strongly dependent upon the sample thermal history (crystallization method) with a peak at 25−26 °C also found.

Ionic Conductivity. The ionic conductivity of the mixtures is shown in Figure 2. The rapid rise in conductivity of the neat ILs (x = 0) is due to the solid crystalline phase melting into a liquid phase. Upon addition of relatively low mole fractions of LiTFSI to PY_{15}TFSI, the onset of melting and the rapid increase in the conductivity occurs at a slightly lower temperature than for the neat IL, in agreement with the lower T_m noted in Figure 1 due to the formation of a eutectic phase. For x = 0.25, however, there is a two step increase in the conductivity for both the PY_{14}TFSI and PY_{15}TFSI mixtures with LiTFSI. From Figure 1, this is attributed to the melting first of the eutectic phase and then the 2/1 IL/LiX (x = 0.33) phase. A dramatic difference exists in the onset of the conductivity increase between the x = 0.25 and 0.33 compositions. This is because the x = 0.33 composition corresponds to the pure 2/1 IL/LiX phase with no eutectic phase present. Samples with a higher LiTFSI concentration also show a conductivity increase at the same temperature due to the melting of this phase. The x = 0.50 sample with PY_{15}TFSI shows a two step increase also due to the melting of the 1/2 IL/LiX (x = 0.67) phase (Figure 2).

At higher temperature (in the melt for all of the samples), the conductivity tends to decrease sharply with increasing LiTFSI concentration for the mixtures with x > 0.10. Steric hindrance shields the positive charge of the PY_{15}^+ cations from the formation of coordination bonds with the neighboring $TFSI^-$ anions, but this is not the case with the Li^+ cations. Each Li^+ cation is coordinated by multiple $TFSI^-$ anions because no solvent is present. Thus aggregates and polymeric ionic chains form, which result in a higher viscosity and lower conductivity as these interactions increase with increasing Li^+ cation concentration.

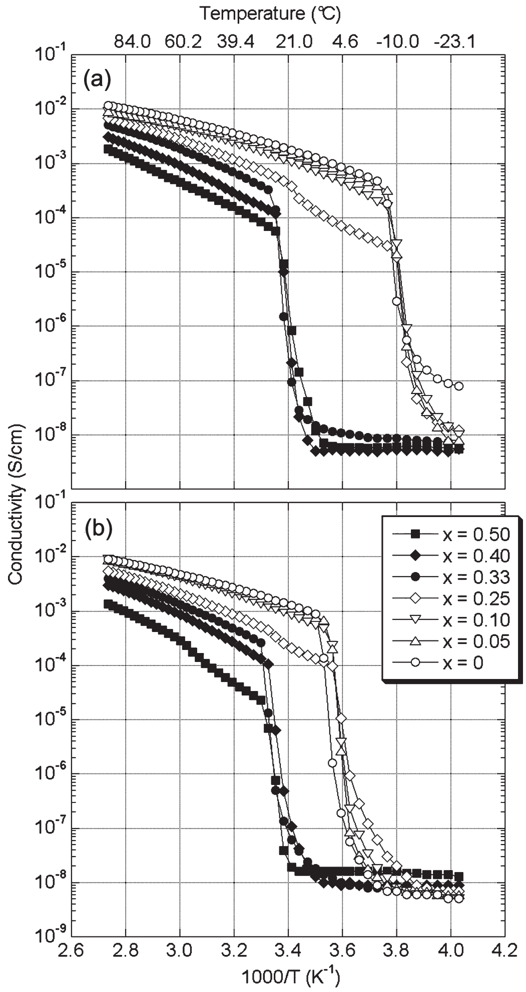

Figure 2. Variable-temperature ionic conductivity of (1−x) PY_{1R}TFSI-(x) LiTFSI mixtures: (a) R = 4 and (b) R = 5.

1/2 PY_{1R}TFSI/LiTFSI (x = 0.67) Crystal Structures. The crystallographic data for the 1/2 (x = 0.67) phases with PY_{14}TFSI and PY_{15}TFSI, respectively, are reported in Table 1 and a schematic illustration of the 1/2 (x = 0.67) PY_{15}TFSI/LiTFSI structure is shown in Figure 3. The $TFSI^-$ anion is known to be flexible, with two low energy conformations with C_1 (cis) and C_2 (trans) symmetry and extensive charge delocalization over the $-SO_2-N-SO_2-$ backbone.[25−27] Both of these conformations are found in the reported crystal structure, as well as intermediate conformations with a dihedral angle of about 70°. The Li^+ cations are coordinated by either 3 or 4 neighboring anions. For the five-coordinate Li^+ cations, two oxygen atoms belong to the same C_2-$TFSI^-$ anion (two oxygen atoms bound to different sulfur atoms on the same $TFSI^-$ anion), two other oxygens belong to a C_1-$TFSI^-$ anion and the last oxygen atom is from a third C_1-$TFSI^-$ anion (Figure 4). Thus, the five oxygen atoms are provided by three $TFSI^-$ anions, one with the C_2 conformation and two with the C_1 conformation. For the 4-coordinate Li^+ cations, each oxygen atom belongs to one $TFSI^-$ anion. Thus, the four oxygen atoms are provided by four $TFSI^-$ anions, two with the C_2 conformation and two with the C_1 conformation (Figure 4).

Table 1. Crystal and Refinement Data

structure	$[PY_{15}TFSI]_1[LiTFSI]_2$	$[PY_{14}TFSI]_1[LiTFSI]_2$
chemical formula	$C_{64}H_{88}F_{72}Li_8N_{16}O_{48}S_{24}$	$C_{60}H_{80}F_{72}Li_8N_{16}O_{48}S_{24}$
fw	4042.46	3986.36
cryst syst	triclinic	triclinic
space group	$P\bar{1}$	$P\bar{1}$
T (K)	110	93(2)
a (Å)	18.4848(6)	18.4561(6)
b (Å)	19.1867(6)	19.2278(7)
c (Å)	22.1063(8)	21.1756(9)
α (deg)	74.5677(19)	75.381(2)
β (deg)	88.853(2)	89.901(2)
γ (deg)	89.2831(18)	89.104(2)
V (Å^3)	7555.9(4)	7270.4(5)
Z	2	2
ρ_{calc} (g cm^{-3})	1.777	1.821
μ (mm^{-1})	0.507	0.526
cryst size (mm^3)	0.42 × 0.24 × 0.03	0.42 × 0.24 × 0.16
$F(000)$	4048	3984
$2\theta_{max}$ (deg)	50.26	50.00
N (R_{int})	165751 (0.0640)	62194 (0.0975)
N [$I > 2\sigma(I)$]	26029	10971
$R_1{}^a$, $wR_2{}^b$ [$I > 2\sigma(I)$]	0.0485, 0.1131	0.0482, 0.0612
$R_1{}^a$, $wR_2{}^b$ (all data)	0.0947, 0.1395	0.1482, 0.0721
GOF^c	1.013	0.786
$\Delta e_{min,max}$ (e Å^{-3})	−0.521, 1.239	−0.571, 0.471

[a] $R_1 = \Sigma||F_o| - |F_c||/\Sigma|F_o|$. [b] $wR_2 = [\Sigma [w(F_o{}^2 - F_c{}^2)^2]/ \Sigma (wF_o{}^4)]^{1/2}$. [c] $GOF = [\Sigma [w(F_o{}^2 - F_c{}^2)^2]/(n - p)]^{1/2}$.

The structure consists of planar sheets of ions formed by a network of anions cross-linked by the Li^+ cations. Cavities in this network each hold two organic $PY_{15}{}^+$ cations. Two of the $PY_{15}{}^+$ cations have similar conformations, while the remaining two have notably different conformations (Figure 4). The ionic sheets are stacked together to form the crystal structure. This structure contains 12 discrete anions that are each coordinated to either 2 or 3 Li^+ cations (Figure 5). A schematic illustration of the 1/2 (x = 0.67) $PY_{14}TFSI/LiTFSI$ structure is shown in the Supporting Information. This structure is isostructural with the structure with $PY_{15}TFSI$ as both structures contain the same cation and anion geometries and the same type of crystal packing, but considerable disorder exists for some of the $PY_{14}{}^+$ cations and $TFSI^-$ anions in the structure with $PY_{14}TFSI$, in contrast with the structure with $PY_{15}TFSI$.

The crystal structure of a 1/2 (x = 0.67) $IM_{102}TFSI/LiTFSI$ phase has been reported ($IM_{102}{}^+$ is 1-ethyl-3-methylimidazolium).[28] The structure is somewhat different from those with $PY_{14}TFSI$ and $PY_{15}TFSI$. In the 1/2 phase with $IM_{102}TFSI$, each Li^+ cation is 5-fold coordinated by anion oxygens from either 3 or 4 different $TFSI^-$ anions. As for the 1/2 phase with $PY_{15}TFSI$, however, the ions form two-dimensional sheets stacked together and cavities are created which accommodate two of the $IM_{102}{}^+$ cations (Figure 3). The crystal structure of a 1/1 (x = 0.50) $IM_{101}TFSI/LiTFSI$ phase has also been reported ($IM_{101}{}^+$ is 1,3-dimethylimidazolium).[29] This structure differs from the 1/2 structures in that planar ionic sheets are not formed. Instead, linear ionic chains form between the $TFSI^-$ anions and Li^+ cations with the organic cations positioned between the chains.

Raman Spectroscopic Measurements. High resolution, variable-temperature Raman spectroscopy provides additional insight into the $TFSI^-$ anion coordination of the mixtures (Figure 6). This anion has a vibrational band in the 730−770 cm^{-1} region which is due to the expansion and contraction of the entire anion.[30] For solvent-separated ion pair (SSIP)

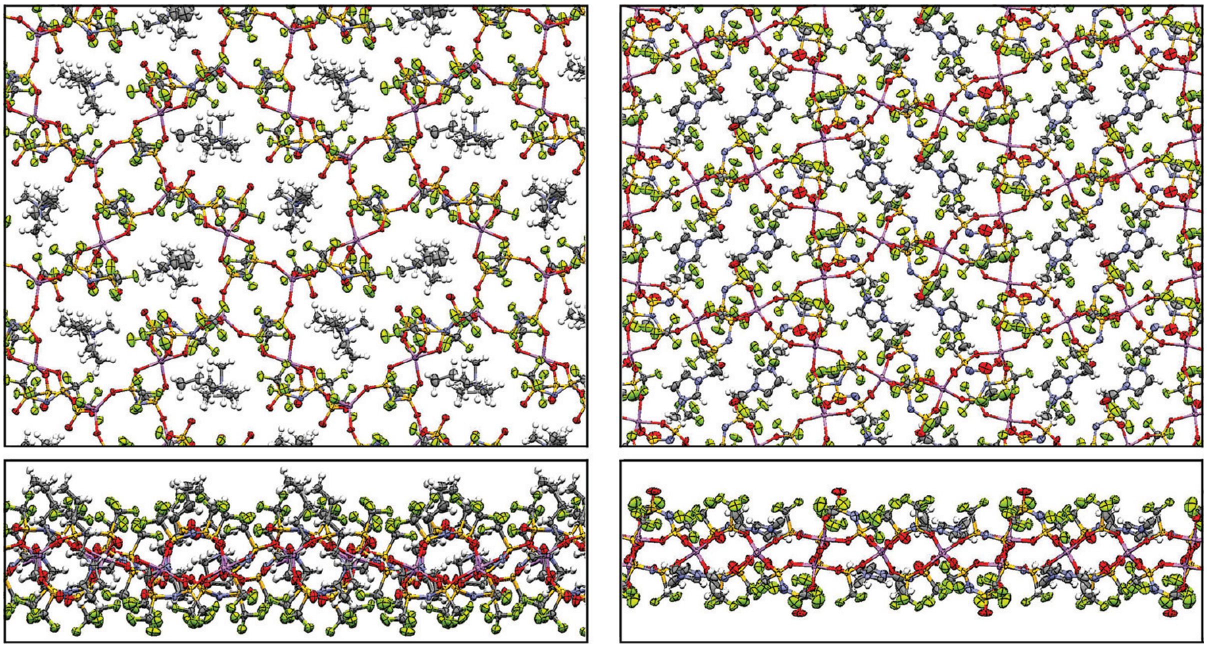

Figure 3. Ion packing in the crystal structure of the (left) (1−x) $PY_{15}TFSI$-(x) LiTFSI (x = 0.67) and (right) (1−x) $IM_{102}TFSI$-(x) LiTFSI (x = 0.67) crystalline phases (two views, rotated 90°) (Li, purple; O, red; S, yellow; N, blue; F, green).[27]

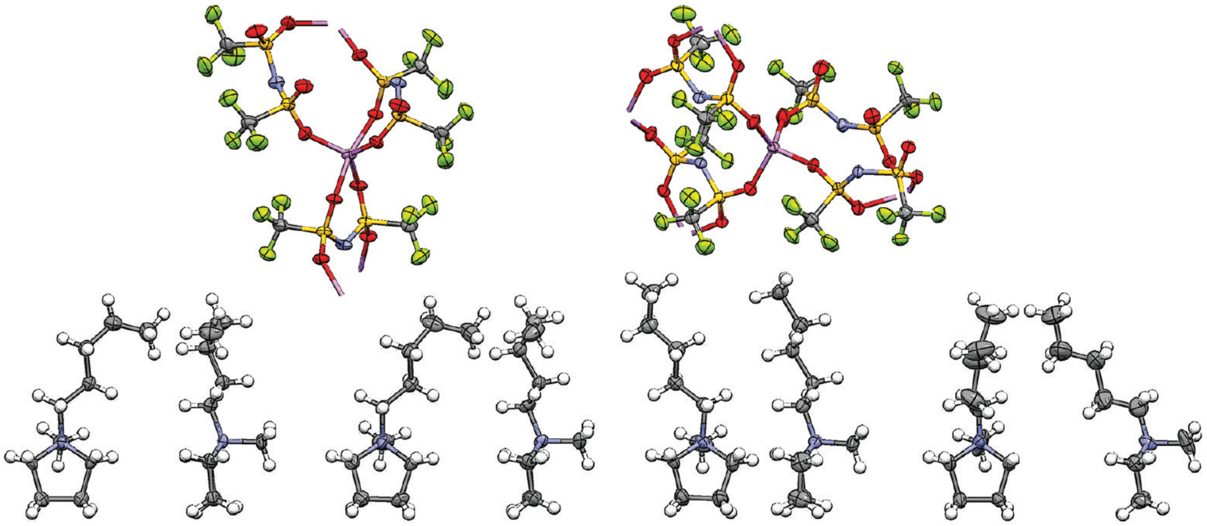

Figure 4. Examples of Li^+ cation coordination by $TFSI^-$ anions and the $PY_{15}{}^+$ cation conformations (2 views shown for each) in the crystal structure of the (1−*x*) PY_{15}TFSI-(*x*) LiTFSI (*x* = 0.67) phase (Li, purple; O, red; S, yellow; N, blue; F, green).

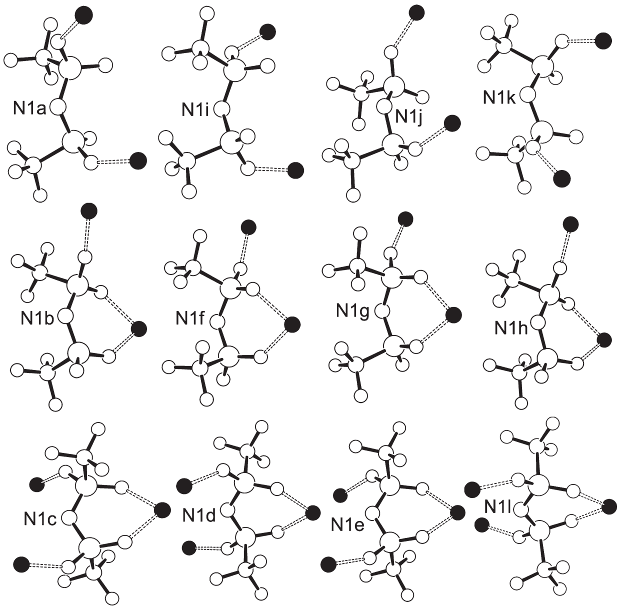

Figure 5. $TFSI^-$ anion coordination to Li^+ cations in the crystal structure of the (1−*x*) PY_{15}TFSI-(*x*) LiTFSI (*x* = 0.67) phase (coordination bonds are dashed and Li^+ cations are black).

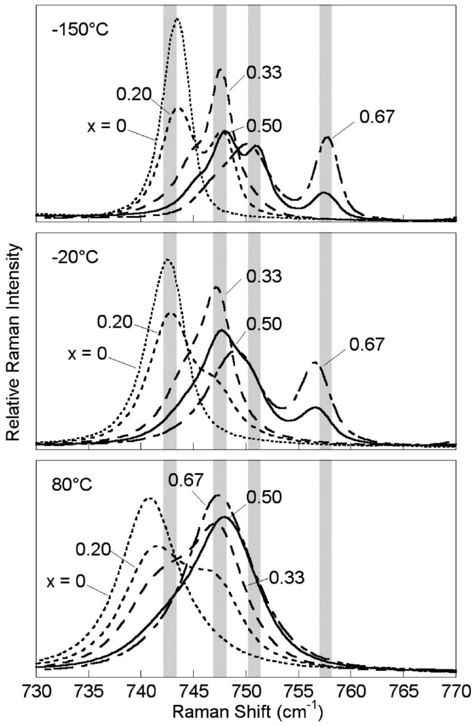

Figure 6. Raman spectra of (1−*x*) PY_{15}TFSI-(*x*) LiTFSI mixtures at different temperatures.

solvates with uncoordinated $TFSI^-$ anions, this band is positioned at approximately 740−744 cm^{-1}.[31−36] If the anion is coordinated through its oxygen atoms to one or more Li^+ cations, however, the band shifts to a higher wavenumber. Assignment of the bands for specific solvate structures is complicated by both the flexibility of the anion and the diversity of ways in which the anion can coordinate one or more Li^+ cations using its four oxygen atoms (Figure 5). In the literature, contact ion pair (CIP) solvates in which the anion is coordinated to a single Li^+ cation are assigned to a band at approximately 747−750 cm^{-1}.[30−35] To aid in the confirmation of these assignments, as well as the band assignments for aggregate (AGG) solvates and pure LiTFSI in which the anion is coordinated to two or more Li^+ cations, a Raman study of crystalline solvates with known structures is underway. Examples of the ion coordination found in crystalline solvates with LiTFSI are shown in Figure 7.[37−41] Preliminary work indicates that the Raman band positions and widths are temperature-dependent with the bands broadening at higher temperature and shifting to lower wavenumber. The band assignments at −100 °C are as follows: SSIPs (741−743 cm^{-1}), C_1-CIP-II (746−747 cm^{-1}), C_2-AGG-Ib (749−750 cm^{-1}), C_1-AGG-IIb (751−753 cm^{-1}), and C_2-AGG-III (748 cm^{-1}) (Figure 7). Unfortunately, a comparison of Figures 5 and 7 shows that none of these forms of ionic association corresponds with the coordination noted for the anions in the 1/2 PY_{15}TFSI/LiTFSI

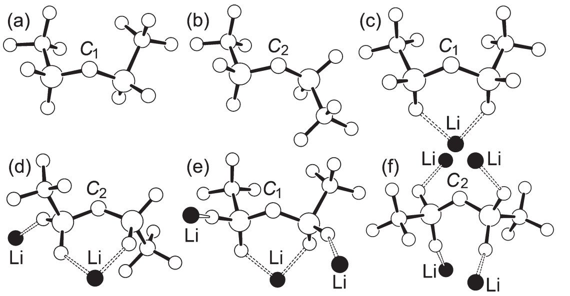

Figure 7. TFSI$^-$ anion coordination to Li$^+$ cations found in crystalline (solvent)$_n$:LiTFSI solvate structures: (a) C_1-SSIP,[35] (b) C_2-SSIP,[36] (c) C_1-CIP-II,[37] (d) C_2-AGG-Ib,[38] (e) C_1-AGG-IIb,[36] and (f) C_2-AGG-III[39] (coordination bonds are dashed and Li$^+$ cations are black; the conformation of the anion is indicated).

phase. For the latter, the ionic association can be classified as C_1-AGG-Ia (C_1 anion coordinated to two Li$^+$ cations through two oxygens), C_1-AGG-Ib (C_1 anion coordinated to two Li$^+$ cations through three oxygens) and C_2-AGG-IIb (C_2 anion coordinated to three Li$^+$ cations through four oxygens). This, combined with the close proximity of some of the vibrational bands with differing forms of coordination, makes it difficult to assign the bands unequivocally. Thus, further structural and Raman characterization of known solvates with LiTFSI is necessary to aid in the deconvolution and assignments of the vibrational bands.

Figure 6 indicates that the pure IL (x = 0) consists only of uncoordinated anions, as expected, due to the steric shielding of the positive charge on the nitrogen of the PY$_{15}$$^+$ cations. Note that the band positions are a function of temperature. The peak position and full-width-at-half-maximum (fwhm) of the band for the uncoordinated anions (x = 0) shifts and broadens with increasing temperature due to increased variability in the anion conformations with increased thermal energy. The x = 0.20 mixture, when crystalline (−150 °C, −20 °C) and in the liquid phase (80 °C), contains both uncoordinated anions and CIP species. The majority of the anions in the x = 0.33 phase appear to be CIPs (anions coordinated to a single Li$^+$ cation, perhaps with two oxygens). It has been suggested from a vibrational spectroscopic analysis that, for low LiTFSI concentrations, $[\mathrm{Li(TFSI)_2}]^-$ species form with bidentate coordinations of the Li$^+$ cations by two oxygen atoms from one anion with a C_2 conformation and two oxygen atoms of another anion with a C_1 conformation.[42] The x = 0.50 sample appears to be a mixture of the coordination for the x = 0.33 and 0.67 samples. The DSC data indicate that there may be a eutectic between these two latter phases which would explain this. The manner in which this sample is crystallized, however, affects the coordination observed. Raman data are provided in the Supporting Information that show it is possible to crystallize this sample to give a prominent peak at 751 cm^{-1} with a corresponding decrease in the peaks at 747 and 757 cm^{-1}. This indicates that, under certain conditions, a different crystalline phase (perhaps a 1/1 PY$_{15}$TFSI/LiTFSI phase) may form rather than a mixture of the 2/1 and 1/2 phases. At −150 °C, the x = 0.67 sample is a crystalline solid with the ion coordination noted above. The Raman data indicate that peaks are present at about 747, 750, and 757 cm^{-1}. Three different forms of anion coordination are found in the structure (Figure 5), but none of these correspond to CIP coordination. Thus, it may be that the C_1-AGG-Ia or C_1-AGG-Ib form of coordination result in a band at 747 cm^{-1} (as is found for the C_1-CIP-II form of coordination). The band at 757 cm^{-1} appears to be a new band not previously reported. This band is only present in the crystalline 1/2 PY$_{15}$TFSI/LiTFSI phase. Interestingly, once this phase melts, the band disappears. It is tempting to therefore assign this to the C_2-AGG-IIb coordination as this form of ion linkage would be the most difficult to maintain in the disordered liquid state.

These data suggest that the initial minimal decrease in conductivity in the liquid phase upon the addition of low amounts of LiTFSI to the ILs may be due to the formation of individual $[\mathrm{Li(TFSI)_2}]^-$ species that do not significantly disrupt the dynamics of the ionic mobility. For such compositions, most of the conductivity is, in fact, due to the uncoordinated ions of the IL. In contrast, a further increase in the LiTFSI concentration results in the formation of larger ionic aggregates (chains and then networks) in which the Li$^+$ cations serve as links or cross-links between the aggregated anions. This increasing aggregation of the ions is the explanation for the rapid decrease in the conductivity (and rapid increase in viscosity) of the mixtures in the liquid state with increasing LiTFSI concentration.

■ CONCLUSION

The thermal phase behavior and ionic conductivity of (1−x) PY$_{1R}$TFSI-(x) LiTFSI mixtures have been examined. Adding LiTFSI initially lowers the T_m of the samples due to the formation of a eutectic composition between the crystalline IL and a 2/1 PY$_{1R}$TFSI/LiTFSI (x = 0.33) phase. Several mixed salt crystalline phases form in these mixtures and the ionic conductivity in all of the crystalline phases is found to be low, but correlates well with the reported phase behavior. The crystal structures for the 1/2 PY$_{1R}$TFSI/LiTFSI phases (R = 4 and 5, x = 0.67) and Raman spectroscopic data provide tremendous insight into the cation−anion coordination and packing in these binary salt mixtures. With increasing concentration of LiTFSI, Li$^+$ cations serve as cross-links between the anions forming aggregates and eventually networks of ions resulting in a dramatic decrease in the ionic conductivity.

■ ASSOCIATED CONTENT

Ⓢ Supporting Information. Experimental data (^{1}H NMR and elemental analysis for PY$_{15}$TFSI and Raman spectroscopic data for the PY$_{15}$TFSI-LiTFSI mixtures) and X-ray crystallographic data files (CIFs) for the 1/2 PY$_{1R}$TFSI/LiTFSI (R = 4 and 5) structures. This material is available free of charge via the Internet at http://pubs.acs.org.

■ AUTHOR INFORMATION

Corresponding Author

*E-mail: whender@ncsu.edu.

■ ACKNOWLEDGMENT

The financial support of the U.S. Army Research Office (ARO) under Contract Grant W911NF-07-1-0556 is gratefully acknowledged.

■ REFERENCES

(1) Ohno, H., Ed. *Electrochemical Aspects of Ionic Liquids*, 2nd ed.; Wiley-VCH: Hoboken, NJ, 2011.

(2) Armand, M.; Endres, F.; MacFarlane, D. R.; Ohno, H.; Scrosati, B. *Nat. Mater.* **2009**, *8*, 621.

(3) Xu, K. *Chem. Rev.* **2004**, *104*, 4303.

(4) MacFarlane, D. R.; Huang, J.; Forsyth, M. *Nature* **1999**, *402*, 792.

(5) Howlett, P. C.; MacFarlane, D. R.; Hollenkamp, A. F. *J. Electrochem. Soc.* **2004**, *7*, A97.

(6) Sakaebe, H.; Matsumoto, H. *Electrochem. Commun.* **2003**, *5*, 594.

(7) Shin, J.-H.; Henderson, W. A.; Passerini, S. *Electrochem. Commun.* **2003**, *5*, 1016.

(8) Shin, J.-H.; Henderson, W. A.; Passerini, S. *Electrochem. Solid-State Lett.* **2005**, *8*, A125.

(9) Shin, J.-H.; Cairns, E. J. *J. Power Sources* **2008**, *177*, 537.

(10) Lux, S. F.; Schmuck, M.; Jeong, S.; Passerini, S.; Winter, M.; Balducci, A. *Int. J. Energy Res.* **2010**, *34*, 97.

(11) MacFarlane, D. R.; Meakin, P.; Sun, J.; Amini, N.; Forsyth, M. *J. Phys. Chem. B* **1999**, *103*, 4164.

(12) Forsyth, M.; Huang, J.; MacFarlane, D. R. *J. Mater. Chem.* **2000**, *10*, 2259.

(13) MacFarlane, D. R.; Sun, J.; Golding, J.; Meakin, P.; Forsyth, M. *Electrochim. Acta* **2000**, *45*, 1271.

(14) Hill, A. J.; Huang, J.; Efthimiadis, J.; Meakin, P.; Forsyth, M.; MacFarlane, D. R. *Solid State Ionics* **2002**, *119*, 154.

(15) MacFarlane, D. R.; Meakin, P.; Amini, N.; Forsyth, M. *J. Phys.: Condens. Matter* **2001**, *13*, 8257.

(16) Huang, J.; Forsyth, M.; MacFarlane, D. R. *Solid State Ionics* **2000**, *136*, 447.

(17) Henderson, W. A.; Passerini, S. *Chem. Mater.* **2004**, *16*, 2881.

(18) Kunze, M.; Jeong, S.; Paillard, E.; Schönhoff, M.; Winter, M.; Passerini, S. *Adv. Energy Mater.* **2011**, *1*, 274.

(19) Castiglione, F.; Ragg, E.; Mele, A.; Appectecchi, G. B.; Montanino, M.; Passerini, S. *J. Phys. Chem. Lett.* **2011**, *2*, 153.

(20) Hayamizu, K.; Tsuzuki, S.; Seki, S.; Fujii, K.; Suenaga, M.; Umebayashi, Y. *J. Chem. Phys.* **2010**, *133*, 194505.

(21) Appetecchi, G. B.; Tizzani, C.; Scaccia, S.; Alessandrini, F.; Passerini, S. *J. Electrochem. Soc.* **2006**, *153*, A1685.

(22) *SAINT, SADABS, XM and XL version 2009.9*; Bruker-Nonius: Madison, WI, 2009.

(23) Altomare, A.; Burla, M. C.; Camalli, M.; Cascarano, G. L.; Giacovazzo, C.; Guagliardi, A.; Moliterni, A. G. G.; Polidori, G. P.; Spagna, R. *J. Appl. Crystallogr.* **1999**, *32*, 115.

(24) Sheldrick, G. M. *SHELXL-97*; University of Göttingen: Göttingen, Germany, 1997.

(25) Rey, I.; Johansson, P.; lindgren, J.; Lassègues, J. C.; Grondin, J.; Servant, L. *J. Phys. Chem. A* **1998**, *102*, 3249.

(26) Johansson, P.; Gejji, S. P.; Tegenfeldt, J.; Lindgren, J. *Electrochim. Acta* **1998**, *43*, 1375.

(27) Xue, L.; Padgett, C. W.; DesMarteau, D. D.; Pennington, W. T. *Solid State Sci.* **2002**, *4*, 1535.

(28) Matsumoto, K.; Hagiwara, R.; Tamada, O. *Solid State Sci.* **2006**, *8*, 1103.

(29) Zhou, Q.; Fitzgerald, K.; Boyle, P. D.; Henderson, W. A. *Chem. Mater.* **2010**, *22*, 1203.

(30) Herstedt, M.; Smirnov, M.; Johansson, P.; Chami, M.; Grondin, J.; Servant, L.; Lassègues, J. C. *J. Raman Spectrosc.* **2005**, *36*, 762.

(31) Brouillette, D.; Irish, D. E.; Taylor, N. J.; Perron, G.; Odziemkowski, M.; Desnoyers, J. E. *Phys. Chem. Chem. Phys.* **2002**, *4*, 6063.

(32) Lassègues, J.-C.; Grondin, J.; Talaga, D. *Phys. Chem. Chem. Phys.* **2006**, *8*, 5629.

(33) Umebayashi, Y.; Mitsugi, T.; Fukuda, S.; Fujimori, T.; Fujii, K.; Kanzaki, R.; Takeuchi, M.; Ishiguro, S. *J. Phys. Chem. B* **2007**, *111*, 13028.

(34) Duluard, S.; Grondin, J.; Bruneel, J.-L.; Pianet, I.; Grélard, A.; Campet, G.; Delville, M.-H.; Lassègues, J.-C. *J. Raman Spectrosc.* **2008**, *39*, 627.

(35) Shirai, A.; Fujii, K.; Seki, S.; Umebayashi, Y.; Ishiguro, S.; Ikeda, Y. *Anal. Sci.* **2008**, *24*, 1291.

(36) Umebayashi, Y.; Mori, S.; Fujii, K.; Tsuzuki, S.; Seki, S.; Hayamizu, K.; Ishiguro, S. *J. Phys. Chem. B* **2010**, *114*, 6513.

(37) Holbrey, J. D.; Reichert, W. M.; Rogers, R. D. *Dalton Trans.* **2004**, 2267.

(38) Henderson, W. A.; McKenna, F.; Khan, M. A.; Brooks, N. R.; Young, V. G., Jr.; Frech, R. *Chem. Mater.* **2005**, *17*, 2284.

(39) Davidson, M. G.; Raithby, P. R.; Johnson, A. L.; Bolton, P. D. *Eur. J. Inorg. Chem.* **2003**, 3445.

(40) Seo, D. M.; Boyle, P. D.; Henderson, W. A. *Acta Crystallogr.* **2011**, *E67*, m534.

(41) Nowinski, J. L.; Lightfoot, P.; Bruce, P. G. *J. Mater. Chem.* **1994**, *4*, 1579.

(42) Lassègues, J.-C.; Grondin, J.; Aupetit, C.; Johansson, P. *J. Phys. Chem. A* **2009**, *113*, 305.